Jurnal Kejuruteraan 35(1) 2023: 223-230
https://doi.org/10.17576/jkukm-2023-35(1)-21

Static Stress Analysis of Membrane Electrode Assembly (MEA) and Gasket in Proton Exchange Membrane Fuel Cell Stack Assembly Pressure

Nurato.Nurato[a,b], Edy Herianto Majlan[a,*], Wan Ramli Wan Daud[a], Teuku Husaini[a] , Masli Irwan Rosli[a], Abu Bakar Sulong[a], Mohd Shahbudin Mastar[a] & Darwin Sebayang[b]

[a]*Fuel Cell Institute, Universiti Kebangsaan Malaysia, 43600 Bangi, Selangor Darul Ehsan, Malaysia*
[b]*Department Mechanical Engineering, Universitas Mercu Buana, Jakarta – Indonesia*

**Corresponding author: edyhm71@gmail.com*

Received 26 November 2021, Received in revised form 29 May 2022
Accepted 30 June 2022, Available online 30 January 2023

ABSTRACT

The proton exchange membrane fuel cell (PEMFC) system was an electrochemical device that generates electricity through the reaction of hydrogen and oxygen without combustion. Proton Exchange Membrane (PEM) stacks typically consisted of components combined into one unit and equipped with suitable clamping torque. This was to prevent reactant gas leakage and minimize the contact resistance between the gas diffusion medium and the bipolar plate. The combined components consisted of a bipolar plate with a flow field, current collector, membrane electrode assembly (MEA), endplate, and gasket. PEMFC performance was measured concerning its power output, which depends on temperature and the operating pressure. Various efforts had been made to determine the optimal compaction pressure and its distribution through simulations and experiments. Therefore, this research analyzed the static stress of membrane electrode assembly (MEA) and gasket in PEMFC stack assembly pressure. The components' geometric dimensions and mechanical properties, such as endplates, current collectors, bipolar plates, MEAs, and gaskets, were combined for electricity. Pressure-sensitive film (Fuji measure film prescale) was also used to visualize contact pressure distribution between the MEA and the bipolar plate. The result showed that the color variation of the pressure film indicates the exact distribution of pressure entering the stacking design and the contact image. In conclusion, the detailed contact pressure distribution was an important influence on heat transfer processes and local electrochemical reactions in cell stacks.

Keywords: Proton exchange membrane fuel cell; stack assembly; pressure distribution; pressure sensitive film

INTRODUCTION

Fuel cells are the most promising alternative energy sources because they are energy converters which convert the chemical energy of a fuel directly and efficiently into electricity through chemical reactions that bring about efficiency, simplicity, low emissions, and great silence (Stolten & Emonts 2012; Bin et al. 2020) . Another outcome of the conversion process is the production of water and heat (Sulaiman et al. 2015 ; Husaini, et al. 2018) making it environmentally friendly. Proton exchange membrane fuel cell (PEMFC) has high power density, low operating temperature, decreased emission, silent operation, easy startup, and quick erasure (Kaytakoğlu & Akyalçin 2007; Garraín et al. 2011; Tsotridis et al. 2015; Mohd Igbal, M. Z et al. 2018). This conversion process has received considerable attention from a wider community, specifically in automotive applications.

The fuel cell stack combines a single PEMFC assembled in series. A paper or porous carbon cloth and solid polymer membrane, which act as the electrode and electrolyte, are formed into one unit membrane electrode assembly (MEA). MEA is fitted with a bipolar plate (BPPs) on both sides, and a gasket is used to protect leakage between joints. All components are tied together with bolts.

The PEMFC stack application has various deformations and pressures, controlled by the material's components and properties. In this case, the impact of clamp pressure on the stack is quite significant. Leaks and other problems may occur at low-pressure assemblies (Rouss et al. 2008), with possible high-pressure damage to the component assembly unit (Taymaz & Benli 2010). with possible high-pressure damage to the component assembly unit reactants in the gas diffusion layer (GDL) are likely to decrease due to high compression, which increases the mass transfer resistance, and indirectly reduces the stack performance (Zhou et al. 2009; Lim et al. 2017).

The pressure given to the stack is identified through a software simulation and can be measured in several ways using a sensitive film (Mason et al. 2012). The pre-scale films are designed with particle size control technology and consist of microcapsules layered in varying degrees of pressure. The films will release the color-forming material in a density corresponding to the specific applied pressure level.

The design of the stack and compression has a significant influence on the distributions of stress that occur in PEMFC, which can affect its service life (Lee et al. 2005; Nitta et al. 2007). According to (Ge et al. 2006 ; Zhou et al. 2009b), the applied pressure during stake installation can also affect electrical conductivity. This is because increase in pressure leads to a rise in electrical conductivity and a decrease in resistance. Therefore, it is important to determine the optimum pressure applied to the stack to obtain PEMFC performance. This research aims to analyze the mechanical behavior of the PEMFC stack, specifically the most sensitive components, such as membrane/GDL and gasket under the binder torque.

METHODOLOGY

A single PEMFC stack was designed and integrated with two current collectors from copper. The composite graphite bipolar plates and flow field were made by CNC machines consisting of a pair of fiberglass endplates and MEA with homemade GDL. Furthermore, gaskets with silicone or PTFE (Polytetrafluoroethylene) were used to prevent leaks in the system. It is also secured with stainless steel bolts using the required torque to prevent the risk of leakage and good electrical connection around the cuttings unit.

Each material has different mechanical properties, such as graphite, soft and hard polymers, and metals, which display different mechanical behaviors when combined into a unit.

a.

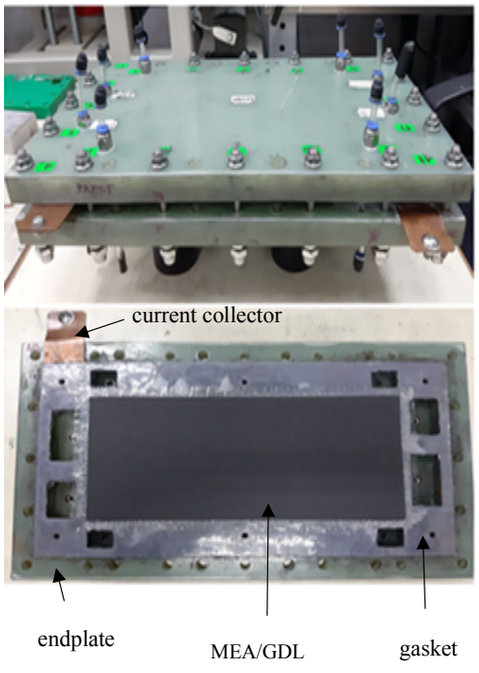

b.

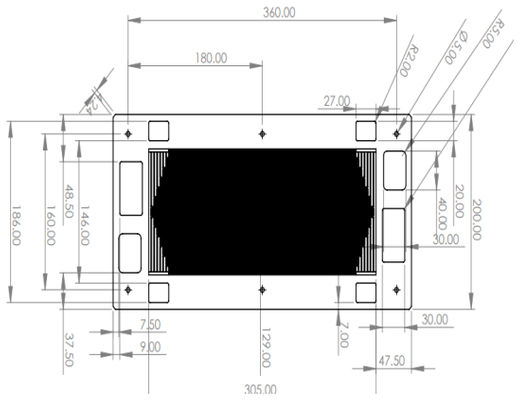

FIGURE 1. a. stack and bipolar plate; b. dimension of bipolar plate in mm

Ansys software with a finite element method was used to simulate the force process on stack assembly arrangement. The loading conditions used are in accordance with the installation pressure torque, which is converted to a force capable of suppressing PEMFC. The power acting on the fuel cell arrangement is the bolt binding force. The force formulas in the reference torque assembly are summarized in equation (Lin et al. 2010).

$$T = F_2 \left[\frac{\delta}{2\pi} + \frac{\mu d}{2} + \frac{\mu_n (D_1^3 - D_0^3)}{3(D_1^2 - D_0^2)}\right] \quad (1)$$

Where T is the assembly torque, F2 is compression force, δ pitch bolt, μ is coefficient friction of nut, d is the nominal diameter of the bolt, D1 is the outer diameter of the nut, D0 is the inner diameter of the nut, and μn is the coefficient of the friction the contact surface.

Bolt tightening can be calculated using the following equation (Childs 2014):

$$T = KF_i d \quad (2)$$

Where T is wrench torque (Nm), K is a constant, Fi is preload (N), and D is the nominal diameter of the bolt.

Von Mises stress is the result of stress analysis from Finite Element Analysis (FEA) obtained in fuel cell arrangement concentrated on torques of 9.8 Nm, 9.3 Nm, 8.8 Nm, 8.5 Nm, and 7.8 Nm, using an M8 bolt. Therefore, from equation, the tightening variations of 4213 N, 3997 N, 3783 N, 3568 N, and 3353 N were obtained.

The simulation used static structural stress analysis to define the overall properties of the material. However, the inability to specify the material will prevent the simulation from functioning. The material assumption is fixed, which means there were no changes due to time and temperature in the property structure. Table 1 shows the components and properties of the material for the simulation.

TABLE 1. Material properties for simulation (Nurato et al. 2019)

Layer	Bipolar Plate	Gasket	Gdl/Mea	EndPlate	Current collector
	Composite	Silicone	Carbon		
Material	Graphite	PTFE	Sheet	Fiberglass	Copper
Dimension (mm)	400x200	400x200	305x129	450x250	400x200
Modulus Youngs (Mpa)	5.60E+04	1.40E+04	4.10E+03	7.20E+04	1.21E+05
Poisson's Ratio	0.17	0.27	0.17	0.21	0.34
Thickness (mm)	1.82	0.5	0.3	24	1.75

The simulation constraints were due to restrictions on movement or model displacement. This research used a constant constraint to curb the model from translation and rotational movements.

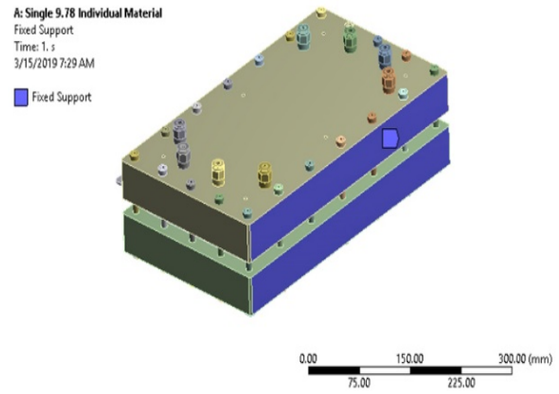

FIGURE 2. Fixed constraint on the fuel cell stacks

Meshing is the division of the object into finite elemental elements with a simpler geometric shape than the "finite element". A meshing process is usually carried out before the process determines the boundary conditions and identifies the loading to the model for analysis. In this research, the mesh bound size for the component was determined by selecting the area determined by the mesh size. Figure 3 shows the cuts for each component comprising 250,370 and 458,003 element and node pieces.

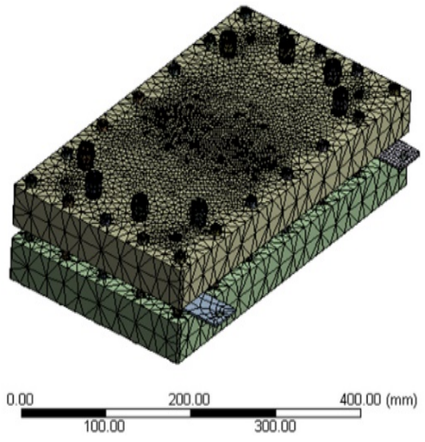

FIGURE 3. Mesh view on the fuel cell stacks

The commercial film-sensitive laboratory (Fuji pre-scale) work is composed of microcapsules filled with color-forming agents. The applied pressure separates these microcapsules, which depends on the pressure value. Therefore, the color-forming agent is released when the microcapsule is solved. This material reacts with the growth to form a magenta color. The pressure-sensitive film has a range of 0 MPa – 2.5 MPa, with the sensors obtained from Fuji and labeled as "Ultra Super Low Pressure". Before the test was performed, sensitive films were tested against the examined pressure and placed between the bipolar plates. The stack was further pumped using the torque lock of the desired torque.

RESULT AND DISCUSSION

The samples from the simulation under load 4213 N as the maximum pressure, deformation, and tension of a single cell are shown in Figure 4. The Von Mises pressure from a single cell (Figure 4a) looked good with a low value. Volts on the surrounding bolts were larger than those at other locations. Furthermore, the voltage was concentrated on unsymmetrical components with complicated profiles, such as current collector, bipolar plate, MEA, and gasket, while the overall symmetry components had low voltage.

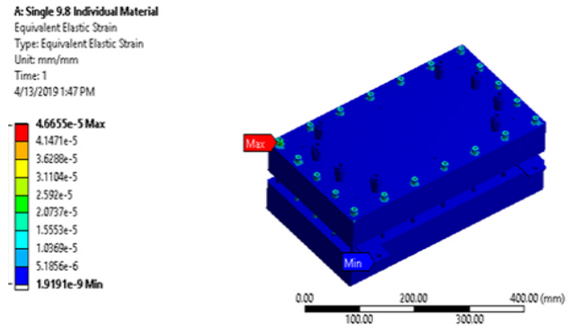

a) Von-mises Stress under force loads of 4213 N

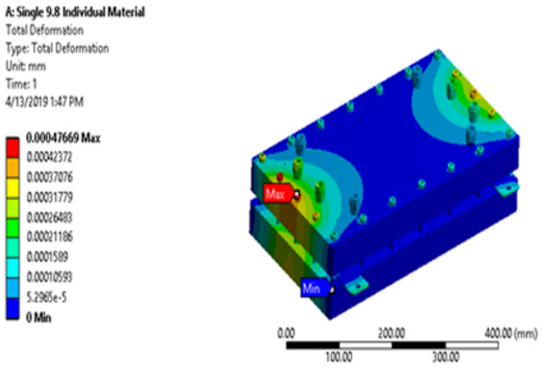

b) Deformation contours under 4213 N

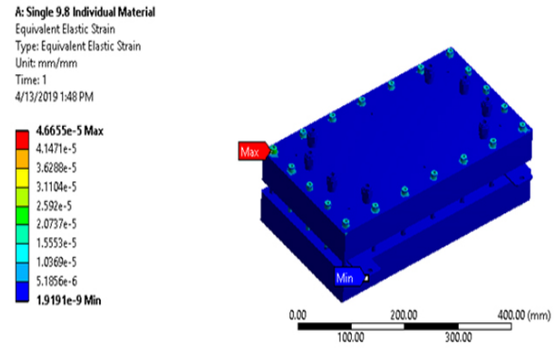

c) Maximum Equivalent Elastic Strain under force loads of 4213 N

FIGURE 4. Contours of Maximum Equivalent Stress, Total Deformation, and the Maximum Equivalent Elastic Strain under force loads of 4213 N.

The simulation results that showed low voltage, deformation, and tension in Figure 3 indicated that the relations among the components were good, hence, the temperature was distributed as a whole. This is in line with the research conducted by (Radhakrishnan & Haridoss 2010; Hu et al. 2018).

Figure 4b showed that the deformation analysis under the tightening bolt 4213 N is below 1.59e-04 mm.

Although the maximum deformation was 4.77 e-04 mm, the biggest change was to the right and left of the single-cell component in the longitudinal direction. According to the research conducted by Hassan et al. (2016), this change of shape was very small. The addition of bolts can significantly reduce the deformation rate that occurs.

TABLE 2. Result summary

Tightening Torque (Nmm)	Applied Force load (N)	Max Equivalent Stress (MPa)	Total Deformation (mm)	Equivalent Elactic Strain Max (mm/mm)
9800	4213	6,49	0,000477	4.665 e-5
9300	3997	6,16	0,000452	4.426 e-5
8800	3783	5,83	0,000428	4.189 e-5
8500	3568	5,49	0,000404	3.951 e-5
7800	3353	5,17	0,000379	3.713 e-5

Table 2 shows that the maximum and minimum bolt tightness occurred in stress variations of 6.49 MPa and 5.17 MPa at 9800 Nmm. Therefore, it can be concluded that this was a parallel connection, where the smaller the bolt tightening strength, the smaller the deformation. Wang et al. (2008) stated that the maximum allowable deformation in a single cell model is 0.2mm, and can be considered very safe with a maximum defect of 4.77E-4 mm. The maximum strain with the largest variation style is 4,665E-5 mm based on simulation results.

The values of 10 different locations in the MEA and gaskets are shown in Tables 3 and 4. In the plot count, locations 1, 2, 3, 8, 9, and 10 were shown as the largest pressure values, while those at 4.5 and 7 were located at the central part of the MEA. The detailed values of 10 MEA stress distribution locations are shown in Table 3. and the maximum strain was 4,665E-5 mm / mm with the largest variation style.

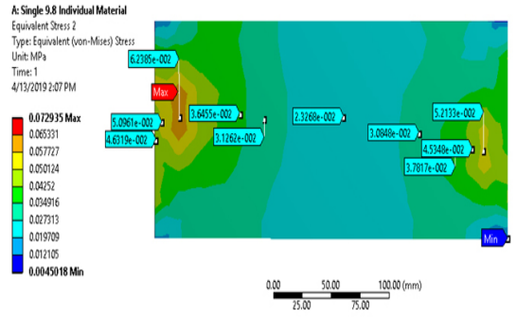

FIGURE 5. Location value in MEA

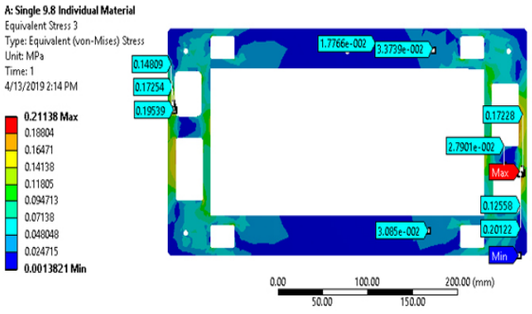

FIGURE 6. Location value in Gasket

The power values that were applied in the MEA were due to a tensile force of 20 pieces. Overall, the simulation results for five types of tightening bolts at the right and left locations in the MEA have the biggest pressure located on the left.

TABLE 3. Maximum equivalent stress MEA

		Assembly Force (N)				
		4213	3997	3783	3568	3353
Simulated Von mises at various locations (MPa)	1	4,63E-02	4,41E-02	4,11E-02	3,96E-02	3,63E-02
	2	5,10E-02	5,05E-02	4,65E-02	4,61E-02	4,19E-02
	3	6,24E-02	5,90E-02	5,53E-02	5,32E-02	4,99E-02
	4	3,65E-02	2,90E-02	3,34E-02	3,14E-02	2,61E-02
	5	3,13E-02	2,24E-02	2,76E-02	2,60E-02	1,95E-02
	6	2,33E-02	2,73E-02	2,14E-02	2,01E-02	2,34E-02
	7	3,08E-02	3,43E-02	2,65E-02	2,61E-02	2,83E-02
	8	3,78E-02	4,32E-02	3,34E-02	3,30E-02	3,15E-02
	9	4,53E-02	4,89E-02	4,18E-02	3,75E-02	3,56E-02
	10	5,21E-02	4,20E-02	4,72E-02	4,47E-02	4,14E-02

Figure 7 shows an example of the stress distributions that occurred in the model under various styles. It can be seen that the entire component had a blue value below 0.04 MPa, while the maximum von Mises pressure tag was 7.29E-02 MPa, with the largest bolt tightening force of 4213 N.

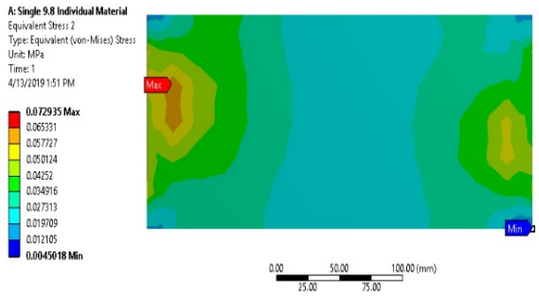

(a) Under force loads of 4213 N

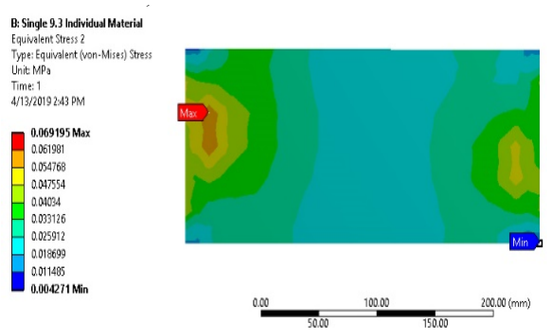

(b) Under force loads of 3997 N

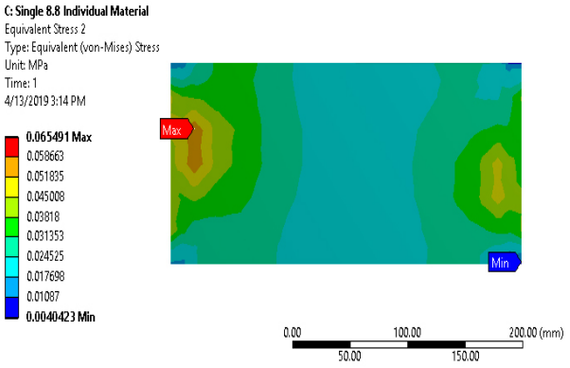

(c) Under force loads of 3783 N

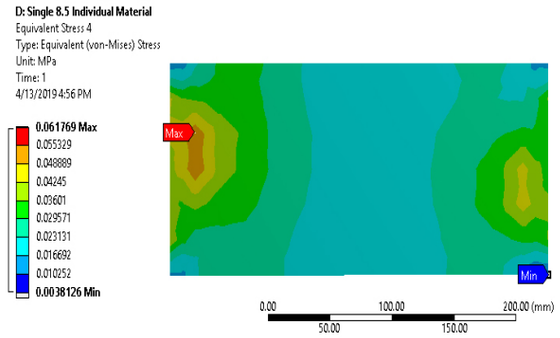

(d) Under force loads of 3568 N

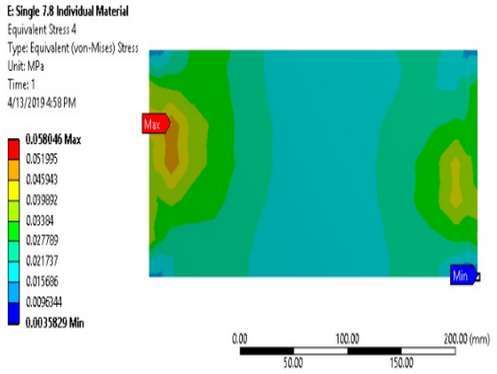

(e) Under force loads of 3353 N

FIGURE 7. Simulated stress distribution plots of the MEA assembly

Table 4 shows a list of voltage simulation results on the gasket component. The maximum value of miser was 2.01E-01 MPa with the largest variation in tightening force. This voltage was located at the right corner of the hole with a drastic profile change. Overall, parts that have changed the profile of component shapes also have a large pressure, as shown in Figure 8. The pressure distribution results are in accordance with Montaini et al. where the gasket supports most of the clamping pressure (Montanini et al. 2009).

The recommended bolt tightening on gasket and MEA is 3353 N with the smallest maximum stress value of 1.58E-01 MPa. I Figure 7 shows that the whole design was valued below 0.1 MPa - 0.2 MPa.

TABLE 4. maximum equivalent stress Gasket

		Assembly Force (N)				
		4213	3997	3783	3568	3353
Simulated Von mises at various locations (MPa)	1	1,95E-01	1,83E-01	1,34E-01	9,89E-02	1,02E-01
	2	1,73E-01	1,68E-01	1,59E-01	1,50E-01	1,21E-01
	3	1,48E-01	1,41E-01	1,77E-01	1,63E-01	1,55E-01
	4	1,78E-02	2,83E-02	1,78E-02	1,40E-02	2,35E-02
	5	3,37E-02	1,91E-02	2,69E-02	2,95E-02	1,42E-02
	6	3,09E-02	3,31E-02	9,59E-02	4,26E-02	2,83E-02
	7	2,79E-02	6,03E-02	1,15E-01	8,97E-02	5,02E-02
	8	1,26E-01	1,17E-01	1,39E-01	1,29E-01	1,19E-01
	9	1,72E-01	1,68E-01	1,59E-01	1,56E-01	1,38E-01
	10	2,01E-01	1,90E-01	1,82E-01	1,71E-01	1,58E-01

This stacking method is effective and recommended for uniform pressure distribution. According to Lee et al (2005), this assembly method creates a non-uniform deformation because the number of bolts used is only four.

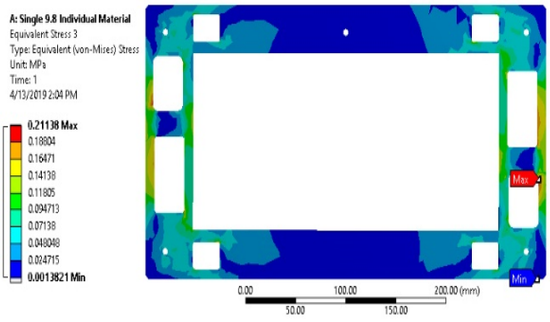

(a) Under force loads of 4213 N

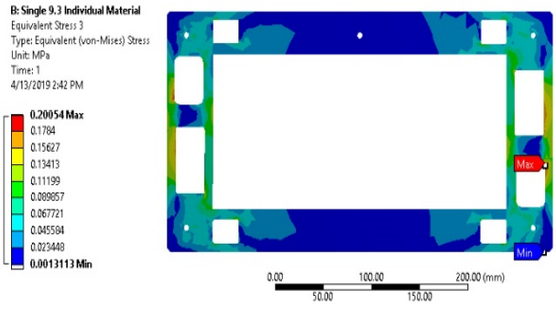

(b) Under force loads of 3997 N

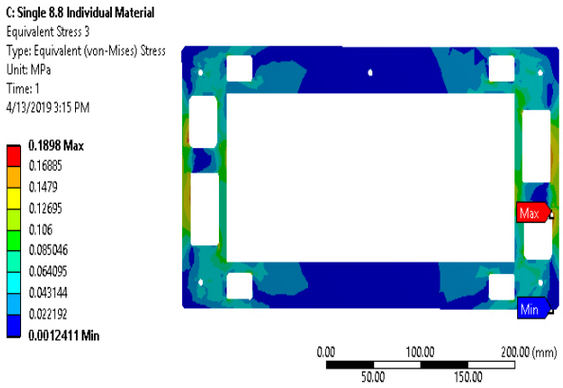

(c) Under force loads of 3783 N

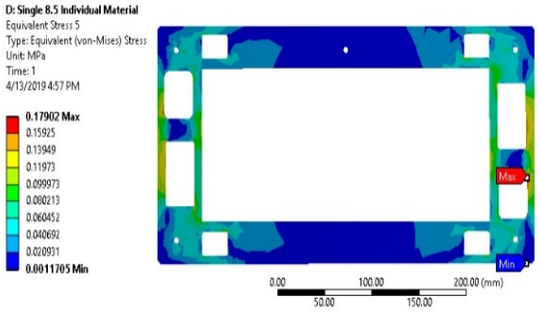

(d) Under force loads of 3568 N

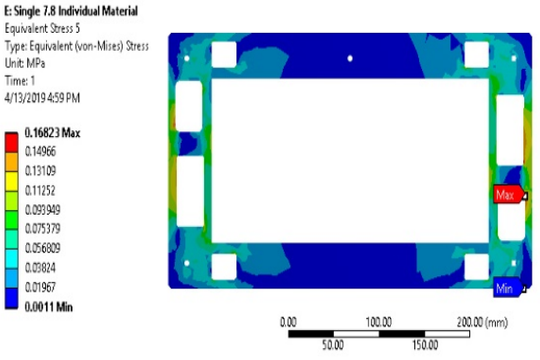

(e) Under force loads of 3353 N

FIGURE 8. Simulated stress distribution plots of the Gasket assembly

Fuji film describes the pressure film as a paper-like sensor used to measure the pressure distributed between two contact objects and the balance in a mono or dual sheet (Https://www.fujifilm.com/products/prescale/prescalefilm/, 2019). Before determining the pressure-sensitive Fuji pre-scale films, the most suitable film type must be chosen. The applicable pressure ranged from type LLLW (ultra super low pressure) to HS (high pressure). Under the influence of external power used, the pre-scale of the film tends to react and emit a magenta color.

The clamping pressure method shown in the pre-scale-sensitive film has varying pressures.

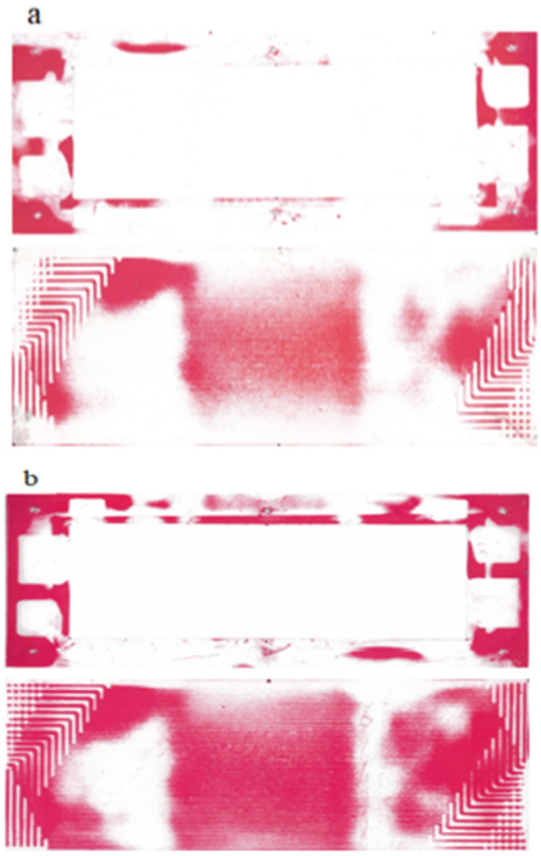

FIGURE 9. pressure sensitive film on gasket and MEA/GDL (a) using 7.8 Nm (b) using 9.8 Nm

Figure 9 shows that the magenta color did not dominate the GDL or MEA layer and gasket. This means that the pressure distribution on the heap was uneven in two conditions. However, this is not in accordance with the simulation process, which exerted inadequate pressure in the middle of GDL.

Uniform pressure distribution on the stack was determined from the simulation results obtained. This research also treated the bipolar plates to ensure they were even with the results shown in Figures 9a and b.

This simulation found that the properties of the material used with the sensitive film act as a guide in treating laboratory components. Finite element methods were used to simulate the assembly of single cells with bipolar graphite plates. These methods were also used to understand the stresses and forms of changes in the FC stack structure. Furthermore, the dimensions and physical properties of the fuel cell components are grouped with the appropriate conduction limit and the actual loading conditions to form a finite element model. A sensitive film was used to determine the actual pressure distribution before installation. From this result, the effect of stack design and cell assembly procedure on stack integration can be evaluated.

This type of simulation helps specify the effectiveness of stack geometry and assembly. The use of simple methods in this analysis is a wise choice to test the validity of the design. Adjustments must be made to the silicone gasket or the stack geometry and bolt configuration. Future models can be developed through decisions and considerations to minimize problems without additional consequences.

CONCLUSION

In conclusion, to investigate the effect of assembly pressure on pem fuel cell performance, theoretical calculations are made to calculate the torque value of the clamp. This was followed by experimental procedures performed to obtain clamping torque for optimal performance. The result showed that assembly pressure can be observed with the use of Fuji-sensitive film and simulation of the software. This analysis recommends using sensibility film to determine the torsion clamping. The use of appropriate materials to generate load pressure and protect sensitive materials is an alternative to maintaining fuel cell durability and its usefulness. Furthermore, detailed contact pressure distribution has an important influence on heat transfer processes and local electrochemical reactions in cell stacks. It is recommended further research need to clarify the role of contact pressure distribution in future stack performance.

ACKNOWLEDGEMENT

The authors acknowledge the financial support provided by the Universiti Kebangsaan Malaysia through the research grants DPK-2021-004.

DECLARATION OF COMPETING INTEREST

None

REFERENCES

Bin, M., Rodin, L., Hasmady, S., Hassan, A. & Zakaria, Z. 2020. *Effect of contamination towards Proton exchange membrane fuel cell performance: A review on experimental and numerical works*. *32*(4), 579–585. DOI:https://doi.org/10.17576/jkukm-2020-32(4)-03.

Childs, P. R. N. 2014. *Mechanical design engineering handbook British library cataloguing in publication data*. http://www.ebooksbucket.com/uploads/engineering/mechanical/Mechanical_Design_Engineering_Handbook.pdf

Garraín, D., Lechón, Y. & Rúa, C. de la. 2011. Polymer Electrolyte Membrane Fuel Cells (PEMFC) in automotive applications: Environmental relevance of the manufacturing stage. *Smart Grid and Renewable Energy 02*(02): 68–74. DOI:https://doi.org/10.4236/sgre.2011.22009.

Ge, J., Higier, A. & Liu, H. 2006. *Effect of gas diffusion layer compression on PEM fuel cell performance*. *159*(May 2005), 922–927. DOI:https://doi.org/10.1016/j.jpowsour.2005.11.069

Hassan, N. U., Kilic, M., Okumus, E., Tunaboylu, B. & Soydan, A. M. 2016. Experimental determination of optimal clamping torque for ab-pem fuel cell. *Journal of Electrochemical Science and Engineering 6*(1): 9–16. DOI:https://doi.org/10.5599/jese.198

Https://www.fujifilm.com/products/prescale/prescalefilm/. (2019). *Prescale*. 1–2.

Hu, G., Wu, X., Suo, Y., Xia, Y., Xu, Y. & Zhang, Z. 2018. Finite element analysis of PEMFC assembling based on ANSYS. *International Journal of Electrochemical Science 13*(2): 2080–2089. DOI:https://doi.org/10.20964/2018.02.60.

Husaini, T., Sulong, A. B. & Muhammad, S. 2018. Effect of temperature on the mechanical performance of highly conductive composites for HT-PEMFC application. *Jurnal Kejuruteraan SI1*(1): 25–30. DOI: https://doi.org/10.17576/jkukm-2018-si1(1)-04.

Kaytakoğlu, S. & Akyalçin, L. 2007. Optimization of parametric performance of a PEMFC. *International Journal of Hydrogen Energy 32*(17): 4418–4423. DOI: https://doi.org/10.1016/j.ijhydene.2007.06.025.

Lee, S. J., Hsu, C. D. & Huang, C. H. 2005. Analyses of the fuel cell stack assembly pressure. *Journal of Power Sources 145*(2): 353–361. DOI:https://doi.org/10.1016/j.jpowsour.2005.02.057.

Lim, B. H., Majlan, E. H., Daud, W. R. W., Rosli, M. I. & Husaini, T. 2017. Numerical analysis of modified parallel flow field designs for fuel cells. *International Journal of Hydrogen Energy 42*(14): 9210–9218. DOI: https://doi.org/10.1016/j.ijhydene.2016.03.189.

Lin, P., Zhou, P. & Wu, C. W. 2010. *A high efficient assembly technique for large proton exchange membrane fuel cell stacks : Part II . Applications 195:* 1383–1392. DOI: https://doi.org/10.1016/j.jpowsour.2009.09.038.

Mason, T. J., Millichamp, J., Neville, T. P., El-Kharouf, A., Pollet, B. G. & Brett, D. J. L. 2012. Effect of clamping pressure on ohmic resistance and compression of gas diffusion layers for polymer electrolyte fuel cells. *Journal of Power Sources 219:* 52–59. DOI:https://doi.org/10.1016/j.jpowsour.2012.07.021.

Mohd Igbal, M. Z., Rosli, M. I. & Panuh, D. 2018. Performance Investigation of High-Temperature Proton Exchange Membrane Fuel Cell. *Jurnal Kejuruteraan SI1*(4): 1–6. DOI: https://doi.org/10.17576/jkukm-2018-si1(4)-01.

Montanini, R., Squadrito, G. & Giacoppo, G. 2009. *Experimental Evaluation of the Clamping Pressure Distribution in a Pen Fuel Cell Using Matrix-Based Piezoresistive Thin-Film Sensor 2039-2044.*

Nitta, I., Hottinen, T., Himanen, O. & Mikkola, M. 2007. Inhomogeneous compression of PEMFC gas diffusion layer. Part I. Experimental. *Journal of Power Sources*, *171*(1): 26–36. DOI: https://doi.org/10.1016/j.jpowsour.2006.11.018.

Nurato, Majlan, E. H., Ramli, W., Daud, W., Husaini, T., Rosli, M. I., Sulong, A. B. & Sebayang, D. 2019. *Finite Element Analysis for Stress Distribution in a Proton Exchange Membrane Fuel Cell Stack*. *7*, 233–240.

Radhakrishnan, V. & Haridoss, P. 2010. Effect of cyclic compression on structure and properties of a Gas Diffusion Layer used in PEM fuel cells. *International Journal of Hydrogen Energy 35*(20): 11107–11118. DOI: https://doi.org/10.1016/j.ijhydene.2010.07.009.

Rouss, V., Lesage, P., Bégot, S., Candusso, D., Charon, W., Harel, F., François, X., Selinger, V., Schilo, C. & Yde-Andersen, S. 2008. Mechanical behaviour of a fuel cell stack under vibrating conditions linked to aircraft applications part I: Experimental. *International Journal of Hydrogen Energy*, *33*(22): 6755–6765. DOI: https://doi.org/10.1016/j.ijhydene.2008.08.032.

Sulaiman, N., Hannan, M. A., Mohamed, A., Majlan, E. H. & Wan Daud, W. R. 2015. A review on energy management system for fuel cell hybrid electric vehicle: Issues and challenges. *Renewable and Sustainable Energy Reviews 52:* 802–814. DOI:https://doi.org/10.1016/j.rser.2015.07.132.

Taymaz, I. & Benli, M. 2010. Numerical study of assembly pressure effect on the performance of proton exchange membrane fuel cell. *Energy 35*(5): 2134–2140. DOI:https://doi.org/10.1016/j.energy.2010.01.032.

Tsotridis, G., Pilenga, A., Marco, G. De. & Malkow, T. 2015. *Eu Harmonised Test Protocols For PEMFC Mea Testing in Single Cell Configuration for Automotive Aplictions.* DOI:https://doi.org/10.2790/54653.

Wang, X., Song, Y. & Zhang, B. 2008. Experimental study on clamping pressure distribution in PEM fuel cells. *Journal of Power Sources 179*(1): 305–309. DOI:https://doi.org/10.1016/j.jpowsour.2007.12.055.

Zhou, Y., Lin, G., Shih, A. J. & Hu, S. J. 2009a. Assembly and performance modeling of proton exchange membrane fuel cells. *Proceedings of the ASME International Manufacturing Science and Engineering Conference 2009, MSEC2009 2:* 723–731. DOI: https://doi.org/10.1115/MSEC2009-84133.

Zhou, Y., Lin, G., Shih, A. J. & Hu, S. J. 2009b. Assembly pressure and membrane swelling in PEM fuel cells. *Journal of Power Sources 192*(2): 544–551. DOI:https://doi.org/10.1016/j.jpowsour.2009.01.085.